Chapter 4

Validation

The simulation of turbulent wall-bounded flows in a channel is a major challenge for any CFD code. The validation of this problem using experimental or DNS as benchmarks is an important step in determining the ability of the turbulence model to handle this type of flow. Large-eddy simulations of two canonical test cases are presented in this chapter for validation purposes. In the cases presented, high-fidelity turbulent DNS results are used as the "gold" standard for measuring the accuracy of our models. DNS is recognized in the community as providing the highest level of turbulent description due to its model-free approach and resolution of the entire scales of motion. Thus, DNS is a reliable computational tool which complements the time trusted methodology of experimental research. Turbulence modeling is applied using implicit grid filtering, dynamic Smagorinsky LES (described in detail in Chapter 2) for momentum and scalar transfer. The first test case corresponds to the classical incompressible turbulent channel configuration. This flow corresponds to a planar, fully developed flow where turbulence develops and sustains itself to form wall-bounded turbulent structures. This configuration has been studied by various researchers for fundamental turbulent validation studies, visualization and modeling purposes and results are compared to the Kim, Moin and Moser test case [1]. The second test corresponds to a similar configuration but with the new complexity of strong temperature gradients at the wall. This adds to the richness of the turbulent physics since it brings in non-passive scalar transport equations in a variable density framework. Results are compared to the DNS data from Nicoud et al [2].

In general, the systematic process of validation has been described as using the right models for a particular study. Validation examines if the conceptual models, computational models as implemented into the CFD code and computational simulation agree with real world observations. The most rigorous strategy is to identify and quantify error and uncertainty through comparison of simulation results with benchmark experimental data. The experiment data sets themselves will contain bias errors and random errors which must be properly quantified and documented as part of the data set. The accuracy required in the validation activities is dependent on the application, and so, the validation should be flexible to allow various levels of accuracy [1]. According to Colemann et al [3], sources of errors and uncertainties in results from simulations can be divided into two distinct sources: modeling and numerical. Modeling errors and uncertainties are due to assumptions and approximations in the mathematical representation of the physical problem (such as mathematical equation, boundary conditions, turbulence models, etc.) and incorporation of previous data (such as fluid properties) into the model. Numerical errors and uncertainties are due to numerical solution of the mathematical equations (such as discretization, artificial dissipation, lack of conservation of mass, momentum, and energy, computer round-off, etc.). Detailed approaches to estimating experimental uncertainties are presented and discussed by Coleman and Steele [3]. Similar systematic validation reports have been studied for major CFD software developed at industry (Boeing, GE, GM) and federal national labs such as Sandia National Labs, NIST, etc. Our focus in this section of the proposal is to validate our simulation results with DNS benchmark data and ensure that the physical trends and majors physical aspects of the flow are accurate. Although, this is not as rigorous as industry based V&V (verification and validation) studies; it does provide a serious level of confidence in the initial state of development of the code.

4.1 Turbulence in channel flow

A classical turbulent benchmark case used to study the mechanics of wall-bounded turbulent flows is the Kim, Moser and Moin configuration originally presented in a landmark paper [1] and extensively referred to in this proposal. The referred work presents a direct numerical simulation of plane turbulent channel flow where all essential scales of motion are resolved. This provides a valuable database for quantitative and qualitative studies of turbulent structure in wall bounded flows and for validation of turbulence closure models.

4.1.1 Wall bounded terminology and resolution requirements

In near wall turbulent flows the viscosity and the wall shear stress are important parameters. Normally a model for the turbulent structure is proposed which consists of two distinct regions, a viscous sublayer and an outer region (log region). The difference in the regions lies in their contributions to the total shear stress profile $\frac{\tau}{\rho} = (\nu + \nu_t)\partial u/\partial y$ where for the viscous sublayer $\nu > \nu_t$ and for the outer region $\nu < \nu_t$. Viscous scales are normally defined based on these quantities for appropriate velocity-scales and length-scales close to the wall. The friction velocity, $u_\tau = \sqrt{\tau_{wall}/\rho}$, and the viscous length scale $\delta_v = \nu/u_\tau$ are used to define the friction Reynolds number as $Re_\tau = \frac{u_\tau \delta}{\nu} = \frac{\delta}{\delta_v}$ where δ is the channel half-height, $\delta = 1$. The distance from the wall in viscous units is defined by $y^+ = \frac{u_\tau y}{\nu}$, also called wall-units, where by inspection we can see that the role of wall-units is similar to a measure of the local Reynolds number. Wall-normal velocity and pressure can also be defined in wall units, in summary:

$$u^+ = \frac{u}{u_\tau} = \frac{u}{\sqrt{\frac{\tau_{wall}}{\rho}}} = \frac{\frac{u}{u_{inf}}}{\sqrt{\frac{C_f}{2}}}, y^+ = \frac{y\,u_\tau}{\nu} = \frac{y\sqrt{\frac{\tau_{wall}}{\rho}}}{\nu} = \frac{y\,u_{inf}\sqrt{\frac{C_f}{2}}}{\nu}$$

$$v^+ = \frac{v}{u_\tau} = \frac{v}{\sqrt{\frac{\tau_{wall}}{\rho}}} = \frac{\frac{v}{u_{inf}}}{\sqrt{\frac{C_f}{2}}}, p^+ = \frac{p-p_\infty}{\rho u_\tau^2} = \frac{\mu\frac{dP}{dx}}{\left(\rho^{\frac{1}{2}}\tau_{wall}^{\frac{3}{2}}\right)}$$

In principle the above normalizations have been used to obtain a universal law of the wall for the viscous sublayer and the outer region (log-region). This is done through integration of the normalized total shear profiles and invoking the classical Prandtl mixing length hypothesis. The results are the law of the wall valid for turbulent boundary layers and channel flows for the case of negligible streamwise pressure gradient.

Law of the wall which states that in the viscous sublayer region (y+ < 5)

$$u^+ = y^+$$

And in the log-law region (y+ > 30)

$$u^+ = \frac{1}{K}\ln(y^+) + B$$

where K = 0.41 is the Von Karman constant and $B = 5.2$ is a turbulent constant.

Wall bounded large-eddy simulations have stringent resolution requirements, similar to DNS, near the wall. This is necessary in order to capture the wall-layer structures that arise when a solid boundary is present. This type of technique is called a “wall-resolved” large-eddy simulation. When designing a turbulent grid for this configuration, one of the objectives will be to spatially resolve the viscous region, log region and the inner layer eddies. In the outer layer,

the important eddies will scale with the boundary layer thickness or characteristic length-scale, like the channel half-height δ, and its resolution should be of order δ. The resolution of the inner-layer is much more demanding since its dynamics are dominated by sweeping and ejecting processes that are generated by the presence (and destruction) of quasi-streamwise vortices. The dimensions of these vortices are constant when normalized in wall-units. Therefore to resolve the sublayer, constant grid spacing in wall units must be used [4]. For channel flows this requirement results in streamwise and spanwise grid sizes of: $\Delta x^+ \cong 100, \Delta z^+ \cong 20$ for spectral methods and half of that for low order finite-difference solvers $\Delta x^+ \cong 50, \Delta z^+ \cong 15$ with both enforcing $y^+_{min} \leq 1$ as suggested by Piomelli [4]. Effective grid design is achieved through hyperbolic stretching in the wall-normal direction, clustering the grids in the inner region and using coarser resolution in the outer region.

4.1.2 Computational domain

Fully developed plane channel flow is homogeneous in the streamwise (x) and spanwise directions (z) and periodic boundary conditions can be used in these directions. The use of periodicity in the homogenous direction is valid as long as the relevant computational dimension is chosen to include the largest eddy in the flow. The periodic domain sizes were originally selected by Kim et al, so that the two point correlations in x and z would be near zero at half the domain size. The pressure gradient that drives the flow is adjusted at every time step to impose a constant mass flux through the channel. This is based on the following conservation equation,

$\left(\frac{dP}{dx}\right)^{n+1} = \left(\frac{dP}{dx}\right)^{n} - 2\left(\frac{\dot{m}^{*n} - \dot{m}}{dt}\right) - \left(\frac{\dot{m}^{*n-1} - \dot{m}}{dt}\right)$ where $\dot{m}^{*n}$ is the calculated mass flux at the current time level and $\dot{m}$ is the required mass flux. The computation is performed using the LES Dynamic Eddy Viscosity model with ~200,00 grid points (48, 65, 64 in x, y, z) with a frictional Reynolds number of 395, based on the frictional velocity and channel half-height. A classical dynamic model, as presented in section 2, is utilized to provide the relationship between Smagorinsky dynamic coefficient and the shear stress. The minimization technique of Lilly (discussed in chapter 2) is used to solve for the dynamic coefficient as presented in Table 1. The streamwise and spanwise computational lengths are chosen to be 2π and π respectively with the channel half-height defined as $\delta = 1$. With this computational domain, the grid spacing in the streamwise and spanwise directions are respectively $\Delta x^{+} = 50$ and $\Delta z^{+} = 15$ in wall units (where $x_i^{+} = x_i\, u_\tau/\nu$), a non-uniform mesh is used in the wall-normal direction where the first point away from the wall is at a distance $y^{+} \cong 1$ and the maximum spacing at the center of the channel is $y^{+} \cong 15$.

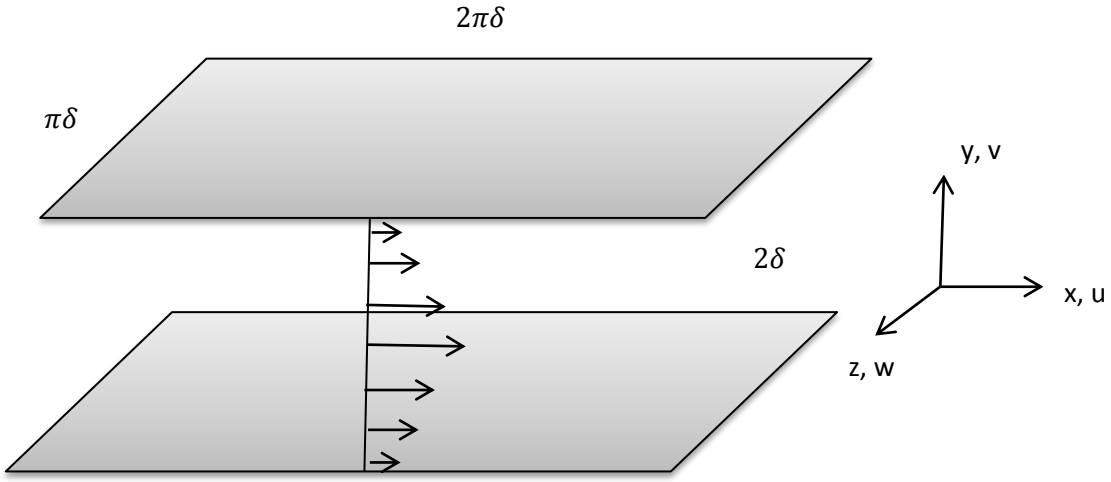

Figure 1. KMM Turbulent Channel Schematic, $Re_\tau = 395$.

Computational Parameter Table

$(L_x L_y L_z)^*$	$(n_x n_y n_z)$	***grid stretching***
$(2\pi\delta, 2\delta, \pi)$	(48,65,64)	- Wall –normal hyperbolic (α= 2.75) - Uniform grid in x, z
Resolution criteria **(finite differences)**	***Turbulence model***	**Turbulent coefficient Minimization technique (Lily, et al)**
$\Delta x^+ \cong 50$ $\Delta z^+ \cong 15$ $y^+ \cong 1$	LES Dynamic eddy viscosity (Smagorinsky type model) $\tau_{ij}^r = -2\nu_t \bar{S}_{ij} = -2C_{ev}\,\Delta^2\,\lvert\bar{S}_{ij}\rvert\bar{S}_{ij}$	$C_{ev}(x,y,z,t) = -\frac{1}{2}\frac{< L_{ij}M_{ij} >_{avg}}{< M_{ij}M_{ij} >_{avg}}$
$Re_{bulk} = 6900$ $Re_\tau = 395$		**Averaging type:** Lagrangian Planar (option) Line (option)
wall boundary	***Mass flux option***	***Periodicity***
$u = v = w = 0$ $T_{wall} = 300K$	Adjust pressure gradient to maintain constant mass flux	Streamwise, Spanwise

Table 1. Computational Parameter Table. KMM turbulent channel case.

4.1.3 Results

The computational study is performed following the parameter table presented in the previous section on Table 1. Initial conditions in the channel are specified with random noise having a magnitude of 40% serving as a kick-start for channel flow instabilities. The flow field variables are integrated forward in time until the flow reaches a statistically steady state. The steady state can be identified by a linear profile of the total shear stress $-\overline{u'v'} + \nu\partial\bar{u}/\partial y$ and by a stationary total kinetic energy. The fluctuations of turbulent kinetic energy serve as a good monitor for the total energy variations in the channel. Thus, the simulation total run time has to include the development of a stationary turbulent kinetic energy history plus several time scales designated large-eddy turn over time (LETOT), $LETOT \sim \frac{\delta}{u_\tau}$. A total of 10 LETOTS were used in this study with 5 measurements taken per time-scale. Thus, the post-processing of the random fields $U_i(x,t)$ is done by performing a temporal average and a spatial average over horizontal planes in the homogeneous directions to obtain the various statistical correlations.

The profiles of the mean streamwise velocity, non-dimensionalized by the friction velocity, is shown in figure 2. Also shown in the figure is the mean velocity profile from the DNS results from Kim, Moser and Moin [1]. The dashed lines represent the law of the wall and the log law. Within the viscous sublayer, $y^+ < 5$, both results follow the linear law of the wall. Similarly in the log-layer, $y^+ > 10$ simulation results show good comparison to the log-law and to the DNS data except for the wake region ($y^+ > 200$) where the peak differences are less than 2 percent.

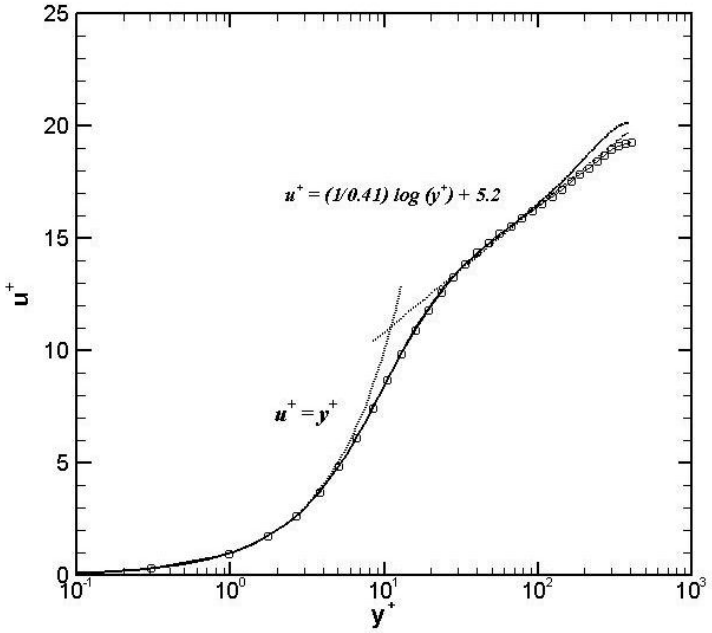

Figure 2. Mean velocity profiles $Re_\tau = 400$. Symbol (ɵ) are current LES simulations and, . ▬ solid black line is reference DNS data, --- dashed lines are the linear and log laws.

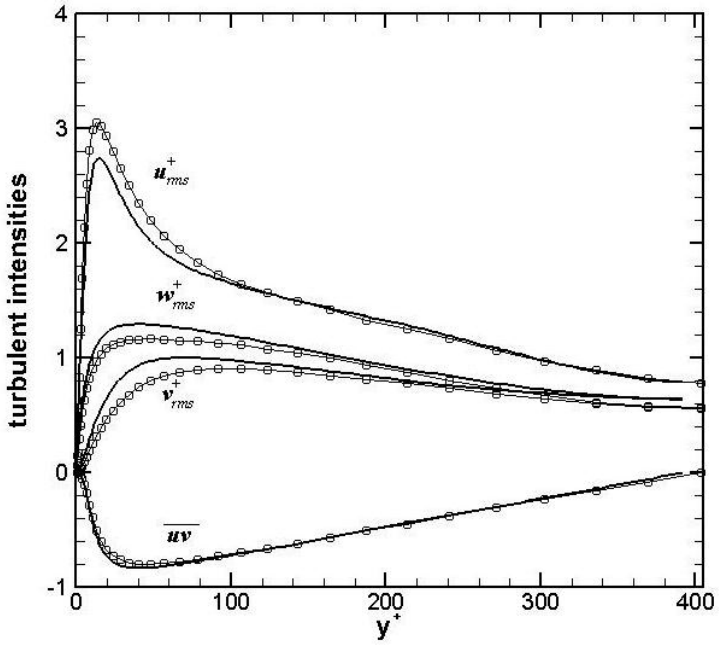

Figure 3. Turbulent intensities of velocity fluctuation normalized by wall shear velocity, $Re_\tau = 400$. Symbol (ɵ) are current LES simulations and ▬ solid black line is reference DNS data.

Turbulent intensities normalized by the frictional velocities are shown in figure 3 and they are compared with DNS results at Reynolds number $Re_\tau = 400$. This is shown up to the centerline of the channel since the profiles are symmetrical. The symmetry of the profiles also shows the adequacy of the sample taken for the average. Although the shape of the profiles agree very well in the wake and log-region, one can still see differences below $y+ \sim 150$ and in particular below the viscous wall region $y^+ < 50$. The modeling of the viscous region is a complex task since it contains the most vigorous turbulent activity. The production, dissipation, turbulent kinetic energy and anisotropy all achieve their peak values at $y^+ < 20$ for flows at high Reynolds numbers [5]. It is due to these phenomena that the modeling errors are most evident in this region. Also shown in figure 3 are comparisons of the Reynolds stress, $\overline{uv}$. Similar to the intensity profiles, the wake and outer region provides the best comparison to the actual turbulence physics. The Reynolds shear stress and its constituents are plotted in figure 4. Due to conservation of mechanical energy and statistical convergence we should expect the total shear stress to be linear across the channel. The behavior of the total shear stress in the vicinity of a wall for a fully developed channel flow can be deduced from the following equation,

$$-\frac{\overline{u'v'}}{u_\tau^2} + \frac{\overline{2\nu_{sgs}S_{ij}}}{u_\tau^2} + \frac{du^+}{dy^+} = 1 - \frac{y^+}{\delta^+}$$

Where the components are: the resolved turbulent stress, the modeled stress and the viscous stress, respectively. The linearity of the conservation property will hold true once we add the total shear constituents. One subtlety encountered in this analysis is that post-processing must include the product of the subgrid-scale eddy viscosity and rate of strain inside the averaging operator due to its spatial and temporal variations in the flow.

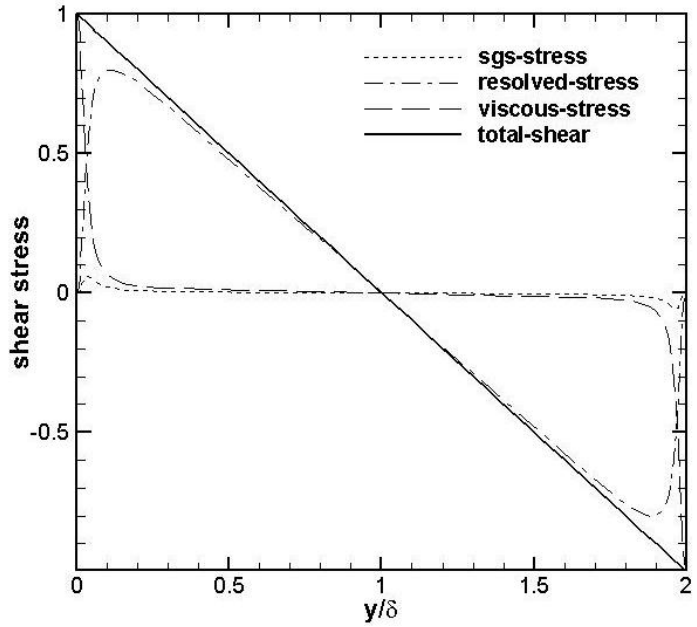

Figure 4. Reynolds shear stress normalized by friction velocity, $Re_\tau = 400$. Solid black line represents the total shear stress (summation of each component) in channel.

Visualization of the flow field is shown on figures 5(a)-(b). Figure 5 presents three dimensional contours of the velocity field showing an instantaneous representation of the turbulent field. To obtain a better representation of the turbulent structure, visualization methods have been developed formulated in terms of the invariants of the velocity gradient tensor $\partial u_i/\partial x_j$ (Where the decomposition of velocity gradient can be made into isotropic, symmetric-deviatoric, and antisymmetric parts: $\frac{\partial U_i}{\partial x_j} = \frac{1}{3}(\delta_{ij} + S_{ij} + \Omega_{ij})$). The Q criterion locates regions where rotation dominates over strain in the flow. Letting S_{ij} and Ω_{ij} denote the symmetric and anti-symmetric parts of $\frac{\partial U_i}{\partial x_j}$, one defines Q as the second invariant of $\frac{\partial U_i}{\partial x_j}$, given as,

$$Q = \frac{1}{2}\left(\Omega_{ij}^2 - S_{ij}^2\right)$$

Where S_{ij} is the rate of strain tensor defined as $S_{ij} = \frac{1}{2}\left(\frac{\partial u_i}{\partial x_j} + \frac{\partial u_j}{\partial x_i}\right)$ and $\Omega_{ij} = \frac{1}{2}\left(\frac{\partial u_i}{\partial x_j} - \frac{\partial u_j}{\partial x_i}\right)$ is the rate of rotation tensor. A coherent vortex is defined as a region where $Q > 0$.

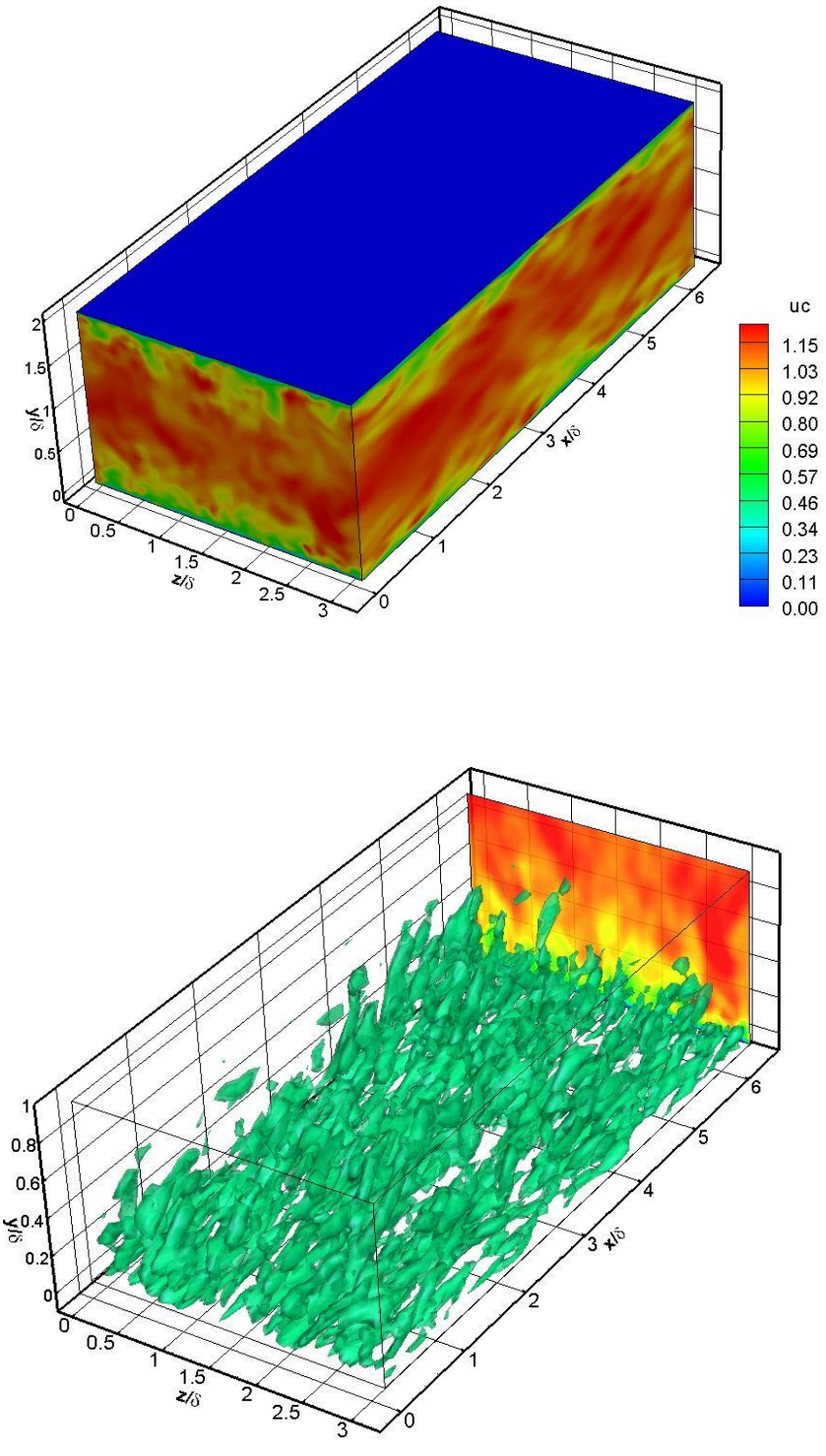

Figure 5.(a) Instantaneous three dimensional velocity contours (b) Turbulent eddy structure presented using the Q-criterion (Q=3) visualization technique --back-plane shows velocity contours.

4.2 Turbulence in channel flow with variable properties

The objective of this section is to validate a turbulence study for the case where thermo-physical properties vary due to strong temperature gradients. This corresponds to a low-Mach number regime where compressibility effects can be neglected ($M < 0.3$) and the effects of variable density based solely on temperature can be studied. Also, of interest is the performance of the large-eddy simulation models in complex cases where large variations in temperature, density and turbulence are coupled.

4.1.1 Wall bounded terminology and resolution requirements

The configuration used in this section corresponds to a planar channel with isothermal walls at different temperatures. In this case the lower wall (designated cold wall) is specified at $T_1 = 300\ K$ and the upper wall (designated hot wall) is prescribed at $T_2 = 600\ K$. A classical Suntherland's law for viscosity is used where $\nu \propto f(T)$ is used based on the reference temperature at the cold wall. In this way, the bulk Reynolds number is defined as $Re_{bulk} = \frac{u_{bulk}\rho_{cold}\delta}{\mu_{cold}}$ where the bulk velocity is $u_{bulk} = \frac{\int \rho(y)u(y)dy}{\int \rho(y)dy}$ (and is also a measure of the channel mass flux) and the values of density and dynamics viscosity correspond to the temperature at the cold wall. A skin friction coefficient, $C_{f_i} = \frac{\tau_{wall_i}}{2\rho_i U^2}$, is also used to characterize the flow at each wall where it is defined based on the mean density in the channel and maximum velocity. We define non-dimensional quantities based on the viscosity, wall shear stress and heat flux. The opposing signs of temperature gradients at each wall indicate that the normalization of dependent variables in viscous units will be anti-symmetrical. The "thermal" viscous units for this case are defined based on the frictional velocity $u_{\tau_i} = \sqrt{\frac{\mu}{\rho_i}\left.\frac{du}{dy}\right|_i}$ and heat flux parameter

$B_{q_i} = \frac{-k_{wall}\frac{dT}{dy}\Big|_i}{\rho_i Cp\, u_{\tau_i}\, T_{wall_i}}$ where the index $i = 1, 2$ indicates the cold or hot wall. Thus the viscous wall units are described by use of the superscript $^+$ as,

$$y_i^+ = \frac{y\rho_i\delta}{\mu_i}\ , \quad u_{\tau\, i}^+ = \frac{u}{u_{\tau_i}}, \quad T_i^+ = \frac{(T_{wall_i} - T)}{B_{q_i} T_{wall_i}}$$

4.2.2 Computational domain

The simulation is performed with periodic conditions applied in the homogenous directions, namely the streamwise (x) and spanwise (z) coordinates. Isothermal walls are specified through the use of Dirichlet boundary conditions prescribing the hot and cold wall boundaries and no-slip conditions specify the non-permeable kinematic wall condition. The pressure gradient is adjusted at every time step to impose a constant mass flux through the channel. The variable density turbulence models developed and implemented are the LES Dynamic Eddy Viscosity and Dynamic Eddy Diffusivity model with classical Smagorinsky type arguments used to describe the relationship between dynamic coefficients, shear stress and heat flux. An extension of the turbulent coefficient minimization scheme is used for the temperature scalars where a Lagrangian averaging option suitable for complex (non-homogenous) flows is utilized. The computational periods and grid details were selected following the suggestion of Nicoud et al [2] where the grid spacing in the streamwise and spanwise directions are respectively $\Delta x^+ = 30 - 50$ and $\Delta z^+ = 8 - 15$ in wall units.

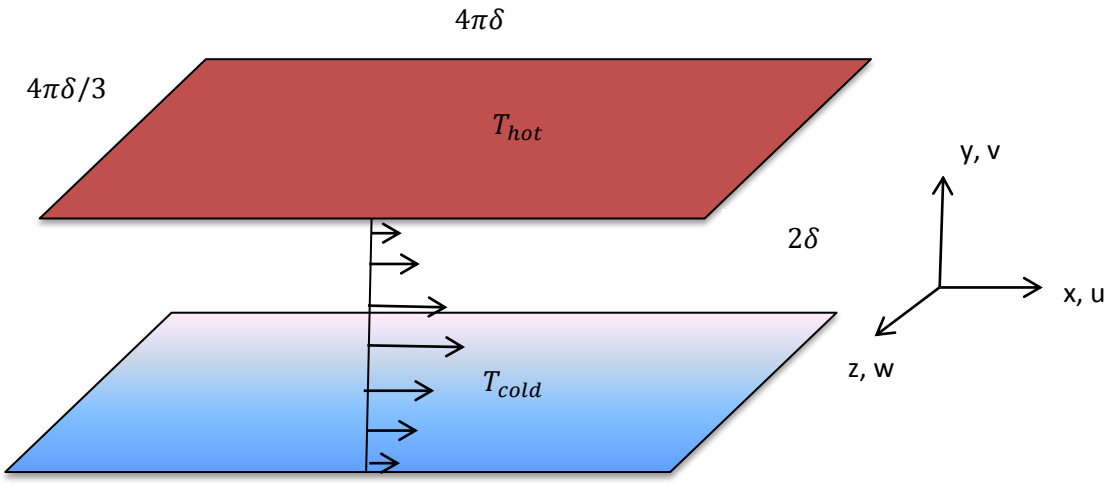

Figure 6. Nicoud Turbulent Channel Schematic

$(L_x L_y L_z)^*$	$(n_x n_y n_z)$	***grid stretching***
$(4\pi\delta, 2\delta, 4\pi\delta/3)$	(48,65,64)	- Wall –normal hyperbolic (α= 2.75) - Uniform grid in x, z
Resolution criteria **(finite differences)**	***Turbulence model***	**Turbulent coefficient Minimization technique (Lily, et al)**
$\Delta x^+ \cong 30 - 50$ $\Delta z^+ \cong 8 - 15$ $y^+ \cong 1$	LES Dynamic eddy viscosity (Smagorinsky type model) $\tau_{ij}^r = -2\nu_t \bar{S}_{ij} = -2C_{ev}\ \Delta^2\ \lvert\bar{S}_{ij}\rvert\bar{S}_{ij}$	$C_{ev}(x,y,z,t) = -\frac{1}{2}\frac{< L_{ij}M_{ij} >_{avg}}{< M_{ij}M_{ij} >_{avg}}$ $C_\theta(x,y,z,t) = \frac{< K_j T_j >_{avg}}{< T_j T_j >_{avg}}$
$Re_{bulk} = 4300$	LES Dynamic eddy diffusivity $q_j = -\overline{\rho} C_\theta \frac{\partial \tilde{T}}{\partial x_j}$	**Averaging type:** Lagrangian Planar (option) Line (option)
wall boundary	***Mass flux option***	***Periodicity***
$u = v = w = 0$ $T_{cold} = 300K$ $T_{hot} = 600K$	Adjust pressure gradient to maintain constant mass flux	Streamwise, Spanwise

Table 2. Computational Parameter Table. Nicoud turbulent channel case

4.2.3. Results

The results presented in this section are generated through a configuration file that follows the parameters presented on Table 2. A kick-start condition of random noise having a magnitude 40% is applied to provide unsteady flow instabilities. The fluctuations of turbulent kinetic energy are closely monitored seeking to obtain a stationary state. The added complexity in this case is the inherent coupling between the scalar and momentum equations and the mixing -time scales provided through heat flux from the isothermal walls. The heat-flux introduces a thermally diffusive component to the heat transfer process that scales like $t \sim \delta^2/D$ and is considerably slower than the convective scales, $t \sim \frac{U}{L}$. This makes the simulation run time substantially longer to obtain a steady profile of kinetic energy. Once this profile is reached a total of ten large-eddy turn over times are used as a total sampling time interval, where five data intervals are recorded per LETOT. Statistical post-processing of the flow-variables is done by performing a temporal average and a spatial average over horizontal planes in the homogeneous directions to obtain the various statistical correlations.

Figures 7(a-b) show that our mean velocity and temperature profile are in good agreement with the DNS results obtained by Nicoud. The non-dimensional velocity profile, Figure 7a, is presented in terms of $\frac{u}{u_{max}}$ along with a dimensional temperature profile shown in Figure 7b. Figure 7b shows that the temperature gradients are larger near the cold wall (at $y = 0$) which through observation indicates the asymmetry in the profile (this asymmetry is also shown in the velocity profile). Note however that through Sundtherland's law, the magnitudes of the heat flux through both walls are approximately the same.

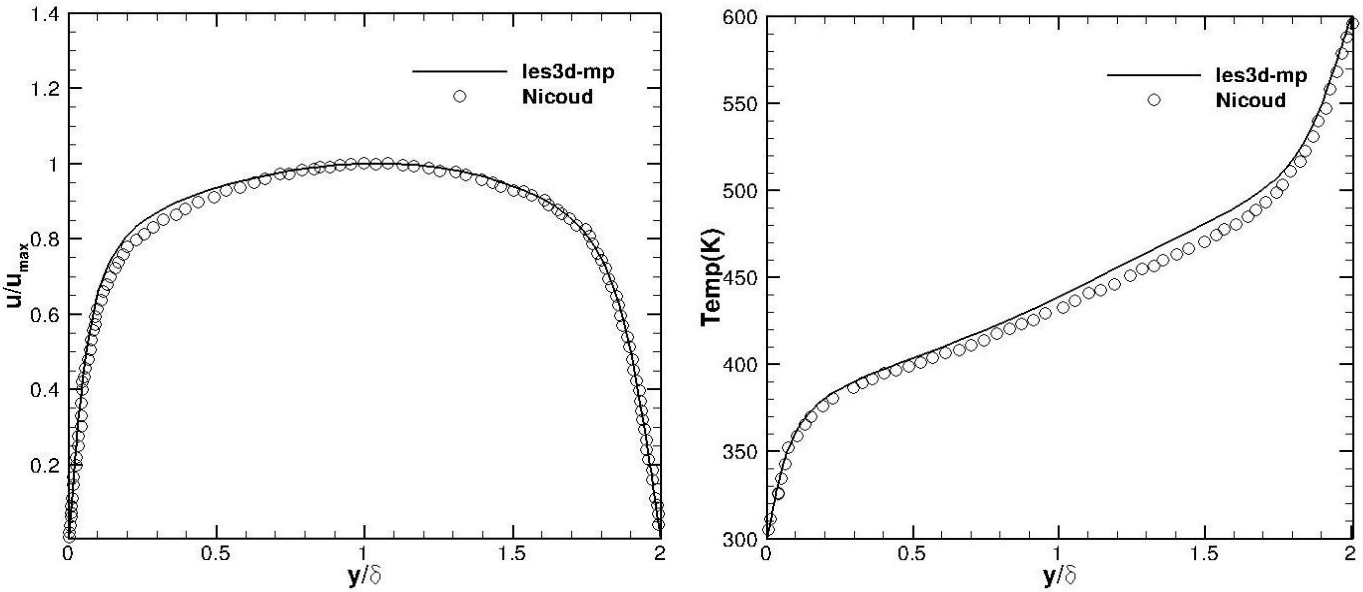

Figures 8 (a-b) show the mean velocity and temperature profiles in viscous thermal wall-units. The results are presented in-terms of cold and hot walls, where the profiles show a different behavior due to variations in thermo-physical properties at each wall in the log-layer, and a similarity as y^+ approaches zero.

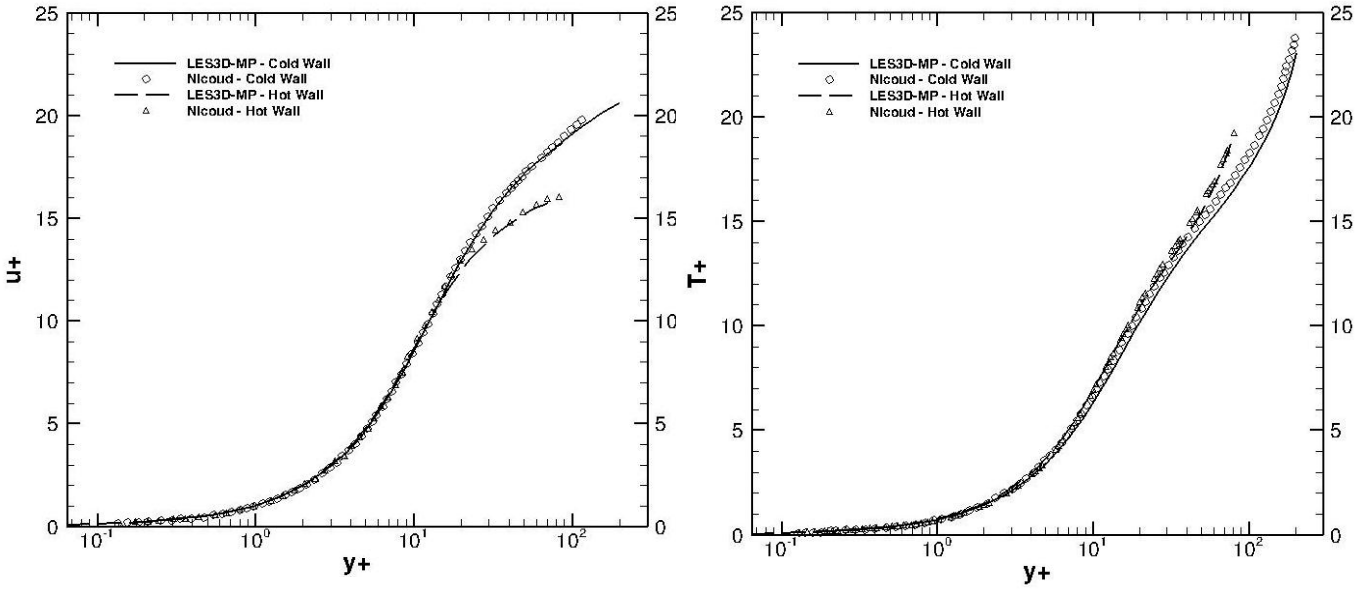

Figure 7. (a) Mean and (b) temperature profiles in thermal viscous wall-units.

Turbulent intensities are shown in Figures 9 (a-b) for streamwise velocity and temperature. Velocity intensities show peak regions of turbulent activity below $y^+ < 50$ for both cold and hot wall. The cold wall shows a larger contribution to both velocity and temperature peak intensities possibly due to presence of larger temperature gradients enhancing turbulent activity.

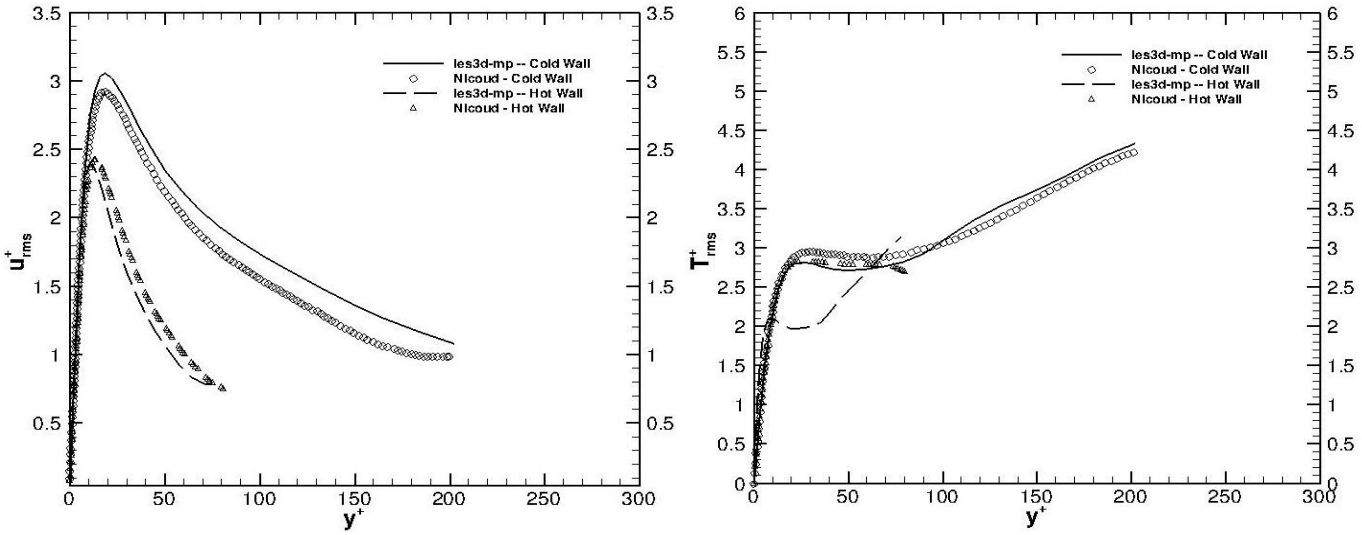

Figure 9. (a) Velocity and (b) temperature turbulent intensities.

Wall-normal and spanwise velocity intensities are presented in Figure 10 (a-b). In contrast to Figure 9, the regions of peak turbulent activity have shifted out to $y^+ \sim 60$ and remain fairly constant beyond this point. Note however that the cold wall peak predominance remains.

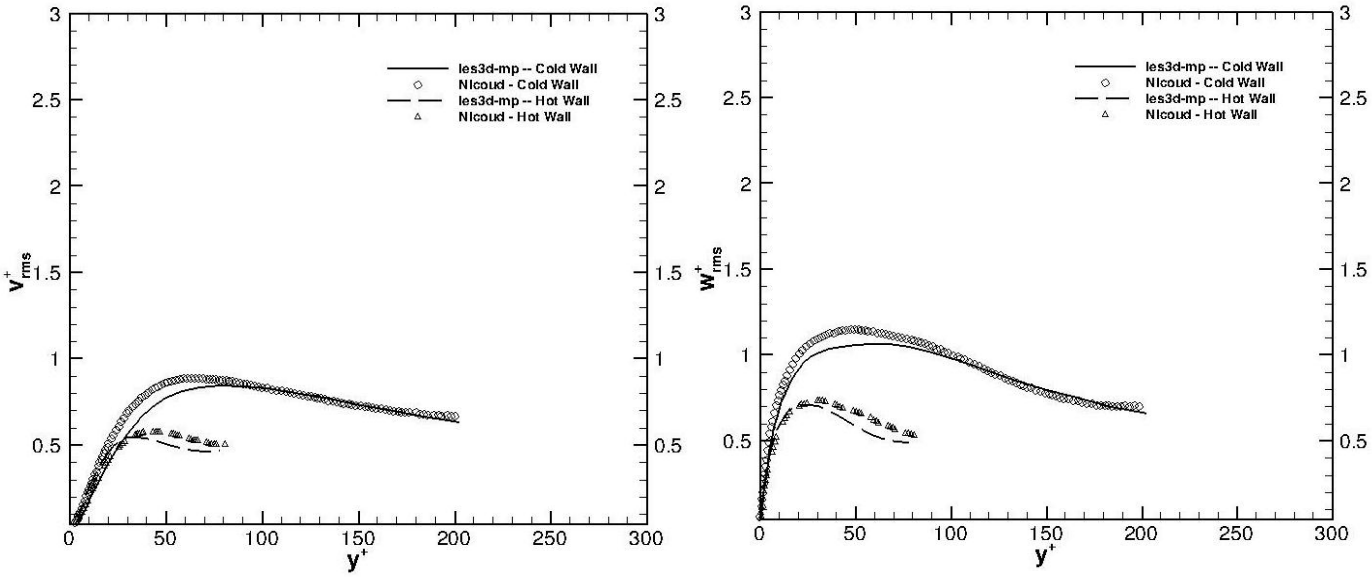

Figure 10. (a) Lateral and (b) spanwise velocity turbulent intensities.

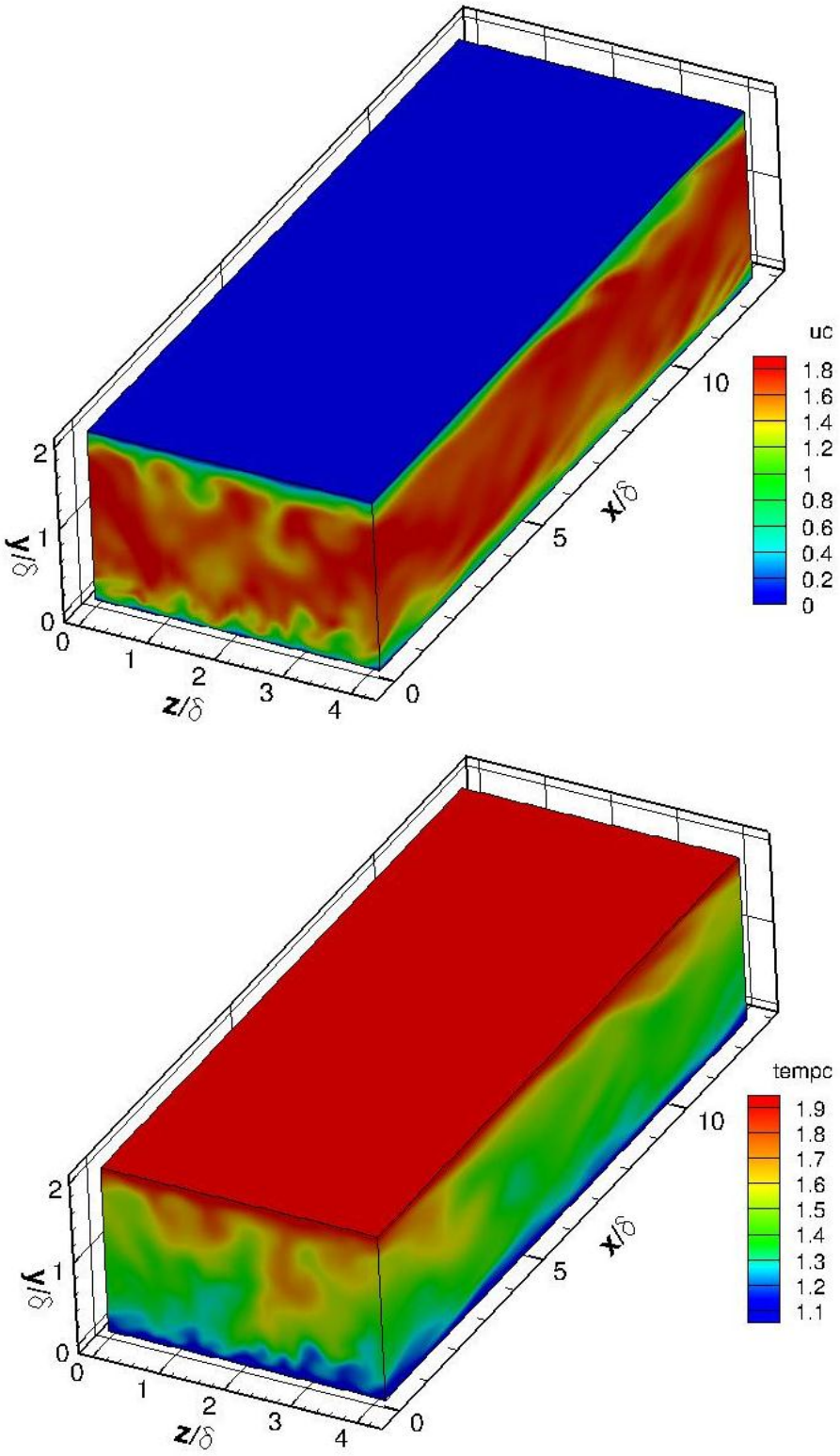

Figure 11. Instantaneous three dimensional (a) velocity contours (b) normalized temperature contours.

Visualization of velocity and temperature flow variables is shown in Figure 11. The pictures present three dimensional contours showing an instantaneous representation of the turbulent field. Close inspection of the near-wall layer shows classical features of boundary layer type flow. Additionally, properties at both the cold and hot wall were calculated and compared to the values provided by Nicoud. This is shown in the following table,

	T_2/T_1	u_{τ_1}/u_τ	u_{τ_2}/u_τ	$C_{f_1}(10^3)$	$C_{f_2}(10^3)$	B_{q_1}	B_{q_2}
LES3D-MP	2	0.87	1.08	6.93	5.30	-0.0177	0.0135
Nicoud	2	0.87	1.13	6.5	5.6	-0.018	0.014

Table 3. Physical property table, Nicoud case.

Table 3 shows good agreement for wall friction velocity and heat flux properties. The ratio of Nicoud's frictional velocity, $u_{\tau_i} = \sqrt{\frac{\mu}{\rho_i}\frac{du}{dy}\Big|_i}$, is in very close agreement with the results obtained with our current LES approach. Similarly, wall heat flux defined as $B_q = \frac{q_w}{\rho_w C_p u_\tau T_w}$ also shows good agreement between both cases. The overall statistical results for mean, turbulent intensities and wall-properties are within reasonable agreement with Nicoud's DNS data. The main discrepancy comes from the intensity profiles whose differences can be attributed to the expected LES modeling errors.

Reference

[1] Moser, Kim, Mansour, “DNS of Turbulent Channel Flow up to Re_tau =590”, Physics of Fluids, vol 11, 943-945, 1999.

[2] Nicoud, F., “Numerical study of channel flow with variable properties”, Center for Turbulence Research, CTR Annual Research Briefs., pp 289-310, 1998.

[3] Coleman, H.W., Stern, F., “Uncertainties in CFD Code Validation”, ASME J.Fluids Eng., Vol. 119, pp. 795-803, 1998.

[4] Piomelli, U., Balaras, E., “Wall-layer models for Large-eddy simulations”, Annual Review of Fluid Mechanics, 34: 349-374, 2002.

[5] Pope, S., “Turbulent Flows”, Cambridge University Press, 2000.